

Article

Behavior of Engineered Cementitious Composites (ECCs) Subjected to Coupled Sustained Flexural Load and Salt Frost

Yonghao Li ¹, Ning Zhang ², Renjuan Sun ^{1,*}, Yanhua Guan ^{1,*}, Lemin Liu ³, Changjin Tian ¹, Yifeng Ling ¹, Hongzhi Zhang ^{1,4} and Branko Šavija ⁵

¹ School of Qilu Transportation, Shandong University, Jinan 250002, China

² Shandong Hi-Speed Engineering Test Co., Ltd., Jinan 250002, China

³ Shandong Expressway Infrastructure Construction Co., Ltd., Jinan 250002, China

⁴ Suzhou Research Institute, Shandong University, Suzhou 215021, China

⁵ Microlab, Faculty of Civil Engineering and Geosciences, Delft University of Technology, 2628 CN Delft, The Netherlands

* Correspondence: sunrenjuan@sdu.edu.cn (R.S.); guanyanhua@sdu.edu.cn (Y.G.)

Abstract: The performance of engineered cementitious composites (ECCs) under coupled salt freezing and loaded conditions is important for its application on the transportation infrastructure. However, in most of the studies, the specimens were generally loaded prior to the freezing. The influence of sustained load was merely considered. To this end, four sustained deflection levels, i.e., 0%, 10%, 30% and 50% of the deflection at the ultimate flexural strength, and three salt concentrations (1%, 3% and 5%) were applied. Prior to the salt frost resistance test, the fluid absorption of ECC specimens under various conditions were measured. The changes in relative dynamic elastic modulus (RDEM) during the freeze–thaw cycles were captured. The depth and the content profile of free chloride were measured after the coupled sustained load and freezing and thawing cycles. It is shown that 3% NaCl solution leads to the largest deterioration in all cases. There is no visible flaking or damage occurring on the surface. The relationships between locally sustained flexural stress and RDEM loss and also locally sustained flexural stress and free chloride penetration depth were proposed and showed satisfactory results. It is concluded that when ECC is subjected to the FTCs under 1% de-ice salt solution, no depassivation of the steel is expected even under a large deflection level. In terms of 3% and 5% salt solution, the thickness of cover should be no less than 20 mm when a deflection level of 0.5 is applied.

Keywords: engineered cementitious composites (ECCs); salt frost; sustained flexural load; chloride penetration depth; free chloride profile



Citation: Li, Y.; Zhang, N.; Sun, R.; Guan, Y.; Liu, L.; Tian, C.; Ling, Y.; Zhang, H.; Šavija, B. Behavior of Engineered Cementitious Composites (ECCs) Subjected to Coupled Sustained Flexural Load and Salt Frost. *Materials* **2023**, *16*, 165. <https://doi.org/10.3390/ma16010165>

Academic Editor: Gwenn Le Saout

Received: 1 December 2022

Revised: 15 December 2022

Accepted: 20 December 2022

Published: 24 December 2022



Copyright: © 2022 by the authors. Licensee MDPI, Basel, Switzerland. This article is an open access article distributed under the terms and conditions of the Creative Commons Attribution (CC BY) license (<https://creativecommons.org/licenses/by/4.0/>).

1. Introduction

Engineered cementitious composites (ECCs) are short-fiber-based cementitious materials [1]. Sometimes they are called strain-hardening cementitious composites (SHCCs) [2] or ultra-high toughness cementitious composites (UHTCCs) [3]. ECCs usually consist of cementitious materials, fine aggregates and fibers. The cementitious materials generally include cement and fly ash [4,5]. It was shown that the incorporation of fibers resulted in excellent mechanical properties [6] and fatigue properties at high fatigue stress and strain levels compared to concrete [7]. Under the action of tension, ECC will exhibit pseudo-strain-hardening and multi-cracking behaviors. The deformation capacity of ECC under tension is much greater than that of plain concrete, which is nearly two orders of magnitude [7]. Furthermore, since ECC has a small crack width, it will have the ability to self-repair in the presence of water [8,9]. Due to its promising properties, ECC has a good potential for use in road engineering. Refs. [10,11] have applied ECC as an overlay on a steel bridge deck and focused on its performance in three-point bending resistance, under wheel axle load and transverse bending, respectively, and the results proved that ECC is eligible as a

cover layer. Furthermore, ECC has been successfully used in a pavement overlay system to eliminate the reflective cracking from the subgrade [12]. It has been reported that, whether in static [13,14] or fatigue flexural conditions [15], the crack width of the ECC layer can be controlled effectively, generally less than 100 μm . So it is difficult for aggressive solutions to enter the interior of the ECC [16,17], resulting in less corrosion and increases in the structure life span.

Prior to the application on road engineering, the durability, e.g., salt frost resistance of ECC, has to be revealed. De-icing salt is usually adopted to reduce road icing and effectively prevent traffic accidents. However, this is a major cause of rapid concrete degradation, causing corrosion of reinforcement, internal cracking and surface scaling [18]. Physico-chemical effects will occur if concrete is in a freeze–thaw environment [19]. It is reported that the internal cracking reduces the dynamic modulus of material and leads to the increase in permeability and porosity [20]. In terms of surface scaling, the damage includes the clearing of fine chips or sheets of objects. It subjects the vulnerable body to moisture and aggressive minerals, threatening the durability [21,22]. Glue-spall theory can be used to explain the scaling mechanism [23,24]. In this theory, the cause of frost salt scaling is the dehiscence of the ice/brine section. The liquid can be classified in three categories, depending on its solute concentration. The concentration of 1–3% is defined as the pessimum salt concentration in which the most severe surface scaling occurs. If the concentration is too low (<0.1%) or high (>10%), no ice cracking or scaling is expected. Furthermore, sodium chloride (NaCl) and other chlorides cause corrosion damage to transportation infrastructure [25,26].

Ref. [27] reported that sodium chloride (NaCl) is used on a large scale for de-icing. Understanding the behavior of ECC under sodium chloride de-icer is, therefore, a key issue for the application of ECC in transportation infrastructure. Liu et al. [28] studied the mechanism of solid waste on the salt freezing resistance of ECC, containing large amounts of fly ash. They showed that the salt-frost-caused degradation is more serious than tap water. Similar observations have been reported in [29]. The presence of fibers can significantly improve the resistance against the progress of scaling by bridging cracks. Van Zijl et al. [30] showed that ECC maintained durability even after freeze–thaw cycles with de-icing salts.

When it is in service, sustained load is applied on ECC. Cracks under sustained load are, therefore, present during the salt frost attack. However, there have been only a few studies taking sustained loading into account. Sahmaran and Li [31] evaluated the durability of ECC with cracks according to ASTM C672. Due to the de-icing salt, the various indicators of specimens are all maintained at an appropriate level even after 50 FTCs with 4% sodium chloride solution. The freeze–thaw durability of pre-cracked ECC in a chloride environment was reported by [32]. However, the research is limited to one stress level and a certain salt solution concentration.

Therefore, this study investigates the effect of salt solution concentration and stress level on the behavior of ECC. NaCl was used as the de-icer and liquids with three concentrations, i.e., 1%, 3%, 5%, were employed for the freezing and thawing cycles. Multiple sustained load levels were used, i.e., deflection at 0, 10, 30 and 50% of ultimate flexural strength. The relative dynamic elastic modulus (RDEM), the depth of chloride penetration and free chloride content were researched. Relationships between locally sustained flexural stress and RDEM loss, as well as locally sustained flexural stress and free chloride penetration depth, were proposed and showed satisfactory results at all salt concentrations.

2. Materials and Methods

2.1. Materials and Specimen Preparation

The materials used include PO42.5 grade cement, class F fly ash, quartz sand, superplasticizer, hydroxypropyl methyl cellulose-based viscosity modifying admixture (VMA) and polyvinyl alcohol (PVA) fiber. Superplasticizer used can reduce water consumption by nearly 40%, and the VMA was used to increase the consistency. PVA fiber was used to improve the

ductility of the matrix. The cement and fly ash were locally produced in Shandong Province, China. The chemical compositions are shown in Table 1. The particle size of quartz sand was between 0.125 and 0.18 mm (80–120 mesh), with a fineness modulus of 0.8. PVA fibers (Kuraray Corporation, Kurashiki, Japan), a length of 12 mm and a diameter of 40 μm being used in this study. The mixture used was developed in a previous study [33] and is shown in Table 2. The mass of water was 0.26 (w/b) of the binder material and the volume ratio of fiber was 2%. The dimension of specimens was 400 mm \times 50 mm \times 25 mm. The stirring process and the curing conditions reference [34]. Prior to the coupled sustained flexural loading and de-icing salt scaling test, except the loaded surface and the one parallel to it, other surfaces of the specimens were sealed using epoxy.

Table 1. Chemical compositions of cement and fly ash (wt.%).

Oxides	CaO	SiO ₂	Al ₂ O ₃	Fe ₂ O ₃	MgO	Na ₂ O	K ₂ O	MnO	TiO ₂	SO ₃	P ₂ O ₅
Cement	63.21	18.48	6.74	3.45	3.24	0.17	0.53	0.27	0.35	3.16	0.16
Fly ash	3.34	49.66	35.97	5.77	0.63	0.62	0.93	0.99	0.04	1.12	0.28

Table 2. The mixture proportions of PVA-ECCs (kg/m³).

Cement	Fly Ash	Quartz Sand	Water	Superplasticizer	VMA	PVA Fiber	W/b
593	712	474	339	4.74	0.55	26	0.26

2.2. Four-Point Bending Test

The test was first applied on the 28 day cured specimen to determine the flexural deformation capacity. The length of the support span and loading span were, respectively, 300 mm and 100 mm. Loading rate of specimen was 0.5 mm/min, this was achieved by the action of a universal testing machine. The mechanical properties were determined by averaging the results from at least 3 specimens.

2.3. Coupled Sustained Loading and De-Icing Salt Scaling Test

Chinese standard GB/T50082-20019 was utilized to evaluate the properties of the loaded ECC under salt freezing conditions. Multiple sustained load levels, namely 0, 10, 30 and 50% of the deflection at the ultimate flexural strength, were used. The construction diagram of the loading device is shown in Figure 1. The specimen was placed between the two loading frames. The supports point distance and loading span were 300 and 100, respectively. The load was applied by twisting the screw. The apparatus and the loaded specimen were placed into a tank with NaCl solution. Three solution concentrations (1%, 3% and 5%) were used.

Before the freezing and thawing cycles (FTCs), specimens were kept in the salt solution for 7 days. The weight of the specimen together with apparatus was measured before and after the saturation to calculate the absorption ability of the specimen. The liquid level was kept 5 ± 1 mm above the bottom of the specimen. The tank was put in a freeze–thaw testing machine with refrigerated liquids. The liquid level was kept 10 ± 1 mm above the bottom of the specimen height. The test was conducted every 12 h as a cycle. In each cycle, temperature was linearly reduced from 20 °C to -20 °C within 4 h, then maintained at -20 °C for 3 h. Afterwards, the temperature was changed linearly to 20 °C within 4 h and maintained at 20 °C for 1 h.

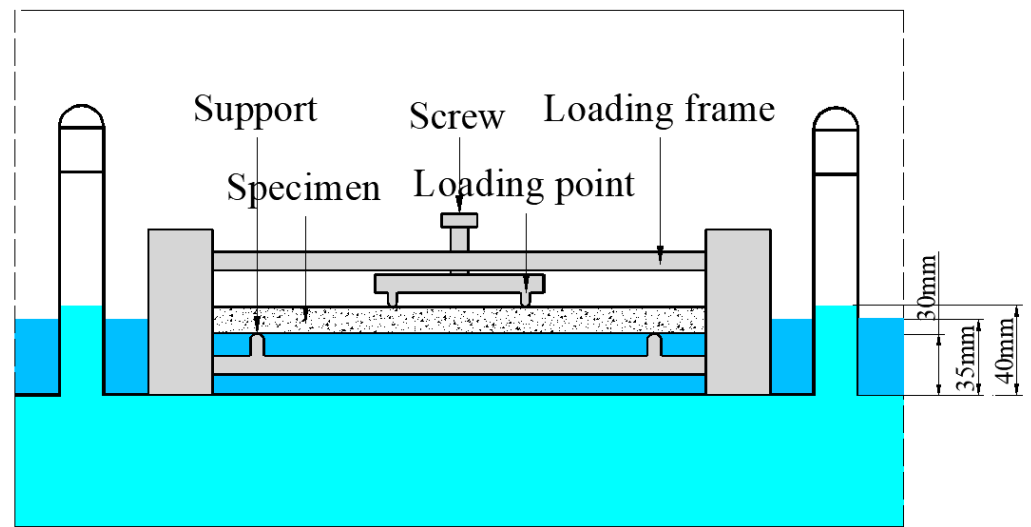


Figure 1. Schematic view of the test configuration.

After every four FTCs, relative dynamic elasticity modulus (RDEM) was measured using ultrasonic waves technique [35]. The longitudinal RDEM was first measured at the two ends of the specimen. The middle part of the two loading points was the pure bending section in which the maximum bending moment was generated. The transversal RDEM was measured at positions A, B, C and D, as shown in Figure 2, which is corresponding to the planes under 0, 0.25, 0.5 and 1 of the maximum bending moment in the pure bending section, respectively. A is the support position, at which the bending moment is 0.

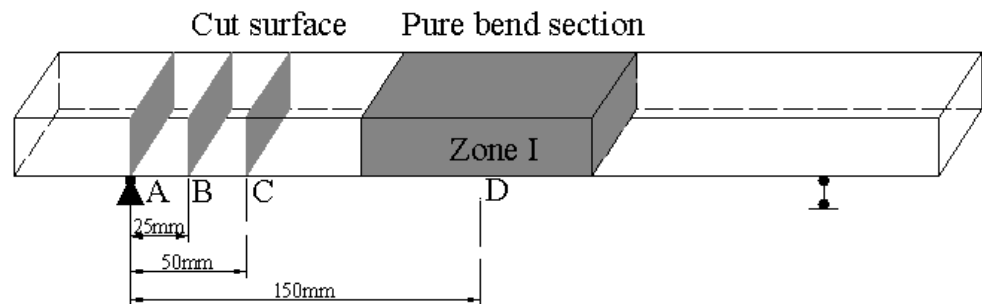


Figure 2. Specimen cutting position.

2.4. Chloride Penetration Depth Measurement

After 28 FTCs, the specimens were removed and cut along planes A, B, C and D (see Figure 2) without water. As a chloride color indicator, 0.1 mol/L AgNO_3 solution was sprayed on the cut surface. In areas where the free chloride concentration is greater than 0.15 wt.% [36], white precipitation occurs. Otherwise, silver oxides with a brown color precipitate [37]. The average depth of the discolored area can be regarded as the chloride penetration depth. The chloride penetration depth was calculated by the white subareas.

2.5. Free Chloride Content Measurement

After 28 FTCs, the specimens were baked under 60 °C for 2 days. The specimen divided by every 5 mm were drilled from the pure bending zone to measure the free chloride content. Samples were made into powder after drying. Powder below 0.15 mm was selected and baked at 60 °C for 1 day. Then, 2% concentration solution with 30 min mixing was prepared for the test.

3. Results

3.1. Flexural Capacity

Load-midspan deflection curve of the 28-day-cured specimen was plotted in Figure 3. The shadow area represents the experimental limits. The different deflection levels are marked with colored dotted lines, and the average of the stresses are indicated by black lines. As anticipated, ECC has demonstrated the deflection hardening behavior [35]. The average ultimate flexural strength is 13.83 MPa, corresponding to a deformation of 10.72 mm. The applied four deflection levels (DLs), namely 0, 0.1, 0.3 and 0.5, were determined as 0 mm, 1.07 mm, 3.22 mm and 5.36 mm, respectively. They correspond to the stress level of 0.59, 0.75 and 0.88, respectively.

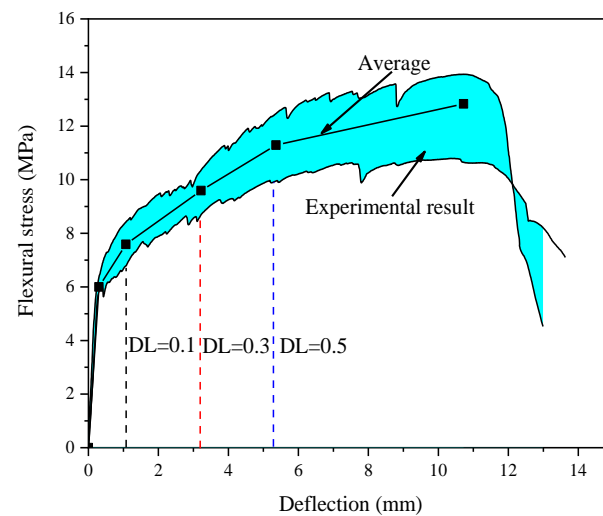


Figure 3. Applied deflection level.

3.2. Fluid Absorption

Figure 4 shows the change of the absorbed fluid over time. The absorption process can be divided into two regimes. Firstly, the specimens absorb fluid rapidly during the initial two days in which the absorbed water accounts for about 80% of the absorbed water. Afterwards, the absorption rate gradually slows down. Clearly, the water absorption increases with the applied deflection, as expected. As the deflection increases, microcracks develop within the specimen causing the specimen to absorb more solution [38]. Furthermore, the absorption increases with the salt solution concentration as salt added the saturation of the ECC [39]. The increment of the absorbed solution between 3% and 5% salt concentrations is smaller than that between 1% and 3% salt concentrations. This is in agreements with the finding reported in [40]. In terms of NaCl solution, 6% concentration leads to the maximum saturation.

Plain concrete absorb approximately 350 g/m^2 after 7 days immersion in 3% NaCl solution, while the water absorption of ECC reaches 957 g/m^2 under the same conditions. This is partly due to the interface formed between PVA fiber and matrix, and the $-\text{COOH}$ and $-\text{OH}$ functional groups in PVA dragging the water molecules forward [41]. Furthermore, as ECC consists of high volume fly ash, the pozzolanic reaction during immersion consumes a large amount of water [42]. At the same time, the addition of the PVA fiber also increases the open porosity, resulting in higher water absorption [43]. Therefore, the absorbed fluid weight of ECC is significantly larger than that of plain concrete.

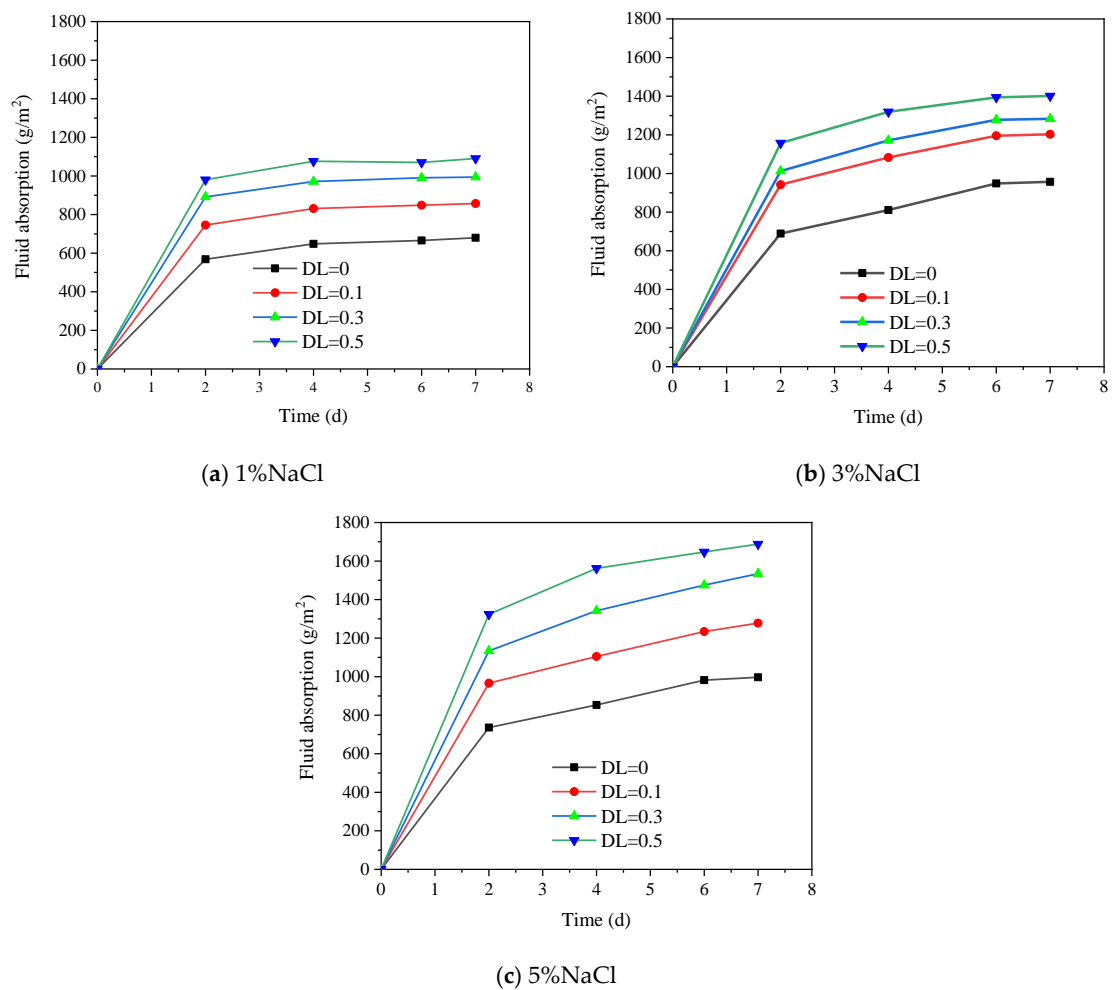


Figure 4. The relationship between water absorption and time for different salt solution concentrations.

3.3. RDEM

3.3.1. Longitudinal RDEM

Figure 5 shows the evolution of longitudinal RDEM along the FTCs. The RDEM decreases with the accumulation of FTCs, indicating that damage or cracks are generated and accumulated inside the material due to the freezing and thawing, and similar results have been presented in [44]. In some cases, the transversal RDEM shows a slight increasing trend within the first 12 FCTs due to the recovered continuity of the materials. The hydration products produced by the ongoing hydration and pozzolanic reaction fills part of the FTCs-induced cracks or the interface between fiber and matrix [45]. However, there is no obvious spalling and damage on the surface, see Figure 6. Cracks were hardly observed in all the specimens, except for the combination with DL = 0.5. It indicates that the cracks produced by the ECC are very fine and may be healed during the freezing and sawing process under the low deflection. At high stress levels, white stuff is present on the crack surface of the specimen. It may be the formation of $\text{Ca}(\text{OH})_2$ and calcium carbonate [46]. Clearly, when the salt concentration is 1%, no change is found and even the specimen is under a relatively large DL. Specifically, after 28 FTCs, the RDEM only decreases 10% for DL = 0.5 in 1% salt solution. This indicates that ECC has a strong resistance to FTCs even under a relatively high stress level of sustained load. Similar results have been reported by [35]. When the salt concentration increases to 3%, a more severe loss of RDEM is observed. This is in accordance with the observation in plain concrete or mortar [47] as the glue-spall stress reaches the maximum at this pessimum salt concentration [24]. With no load, the loss of RDEM is about 5%. Nevertheless, the loss of RDEM is much lower compared with plain

concrete [48] in which the loss of RDEM reaches 20% when exposed to a similar condition in just 16 cycles. This is because fibers can effectively resist the expansion pressure generated by the freezing. Meanwhile, the fiber introduces flaws into the matrix, which is beneficial for frost resistance [49].

The sustained load accelerates the deterioration process as it is shown that the loss of RDEM increases with DL. In case of 3% salt concentration, when DL = 0.5, the RDEM loss reaches 14.38%, which is 10.46% higher than the 3.92% of DL = 0. Moreover, the role of the DL on the deterioration is more significant for the solution with 3% salt concentration. This can be explained to the crack of brine ice formed in the pessimum salt concentration (3%) [24]. The RDEM losses are 2.39% and 9.73% in 1% and 5% salt solutions, which are 11.99% and 4.65% smaller than that of 5% salt solution (14.38%), respectively. Although specimens in 5% salt solution absorb more fluid, the pressure and the volume of solutions are decreased with increasing concentration [50]. Therefore, the most serious deterioration is observed in 3% salt solution.

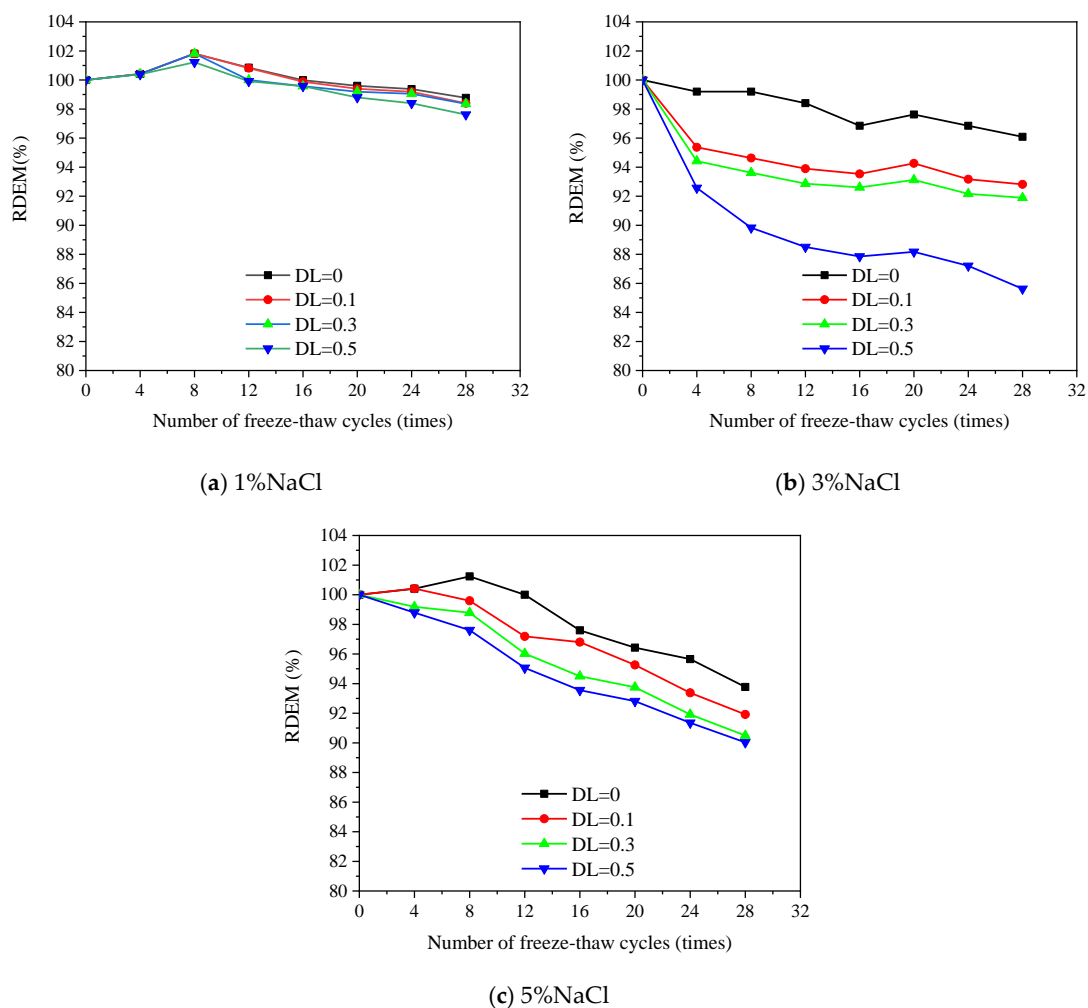
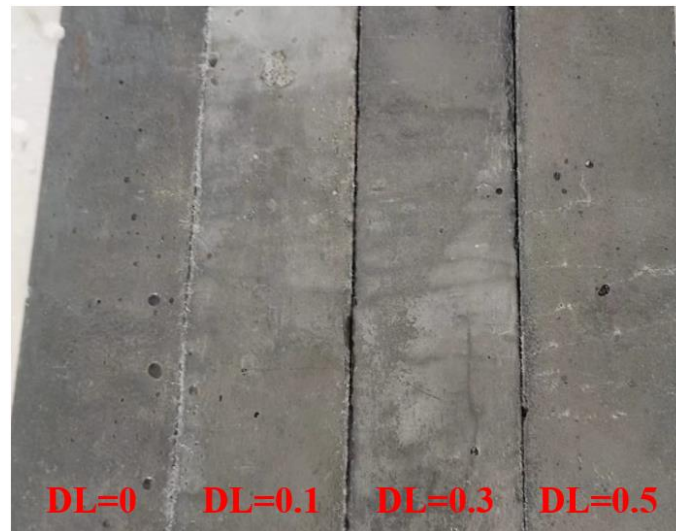
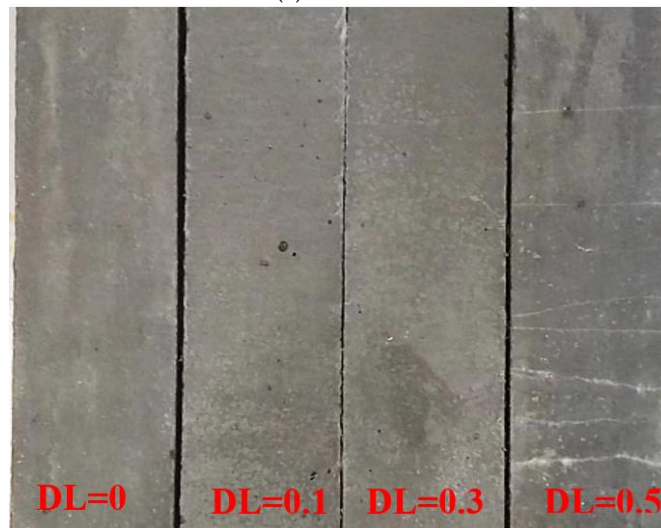


Figure 5. Evolution of longitudinal RDEM along the FTCs under various salt concentrations.



(a) 1% NaCl



(b) 3% NaCl



(c) 5% NaCl

Figure 6. Surface of specimens after 28 FTCs under different salt concentrations.

3.3.2. Transversal RDEM

Figures 7–9 show the evolution of the transversal RDEM at various positions along the FTCs for 1%, 2% and 3% salt solutions, respectively. The flexural stress levels at positions A, B, C and D correspond to 0, 0.25, 0.5 and 1 of the applied maximum flexural stress at the pure bending zone. The loss of transversal RDEM is no more than 10%, which is obviously lower than the longitudinal one. In the same manner as the longitudinal one, the slight increment in the first 12 FTCs is observed for the transversal RDEM.

The loss of transversal RDEM after 28 FTCs and the local flexural stress is plotted in Figure 10. It clearly shows that the RDEM loss and flexural stress can be expressed as a linear relationship. The following equation was, therefore, proposed:

$$y = y_0 + a\sigma \tag{1}$$

where y is the RDEM loss (%), σ is the flexural stress (MPa), y_0 is the RDEM loss with no stress, a is the fitting constant denoting the influence of the flexural stress on the RDEM loss. The fitting shows satisfactory results as the determination coefficient (R^2) is higher than 0.95 for all cases. The value of a is almost the same for the 1% and 5% salt solutions, indicating that the influence of flexural stress on the deterioration for the two concentration is more or less the same. Flexural stress is more significant for the transversal RDEM loss when the specimen is subjected to 3 % salt solution, i.e., the pessimum concentration. This is consistent with the observation of longitudinal RDEM.

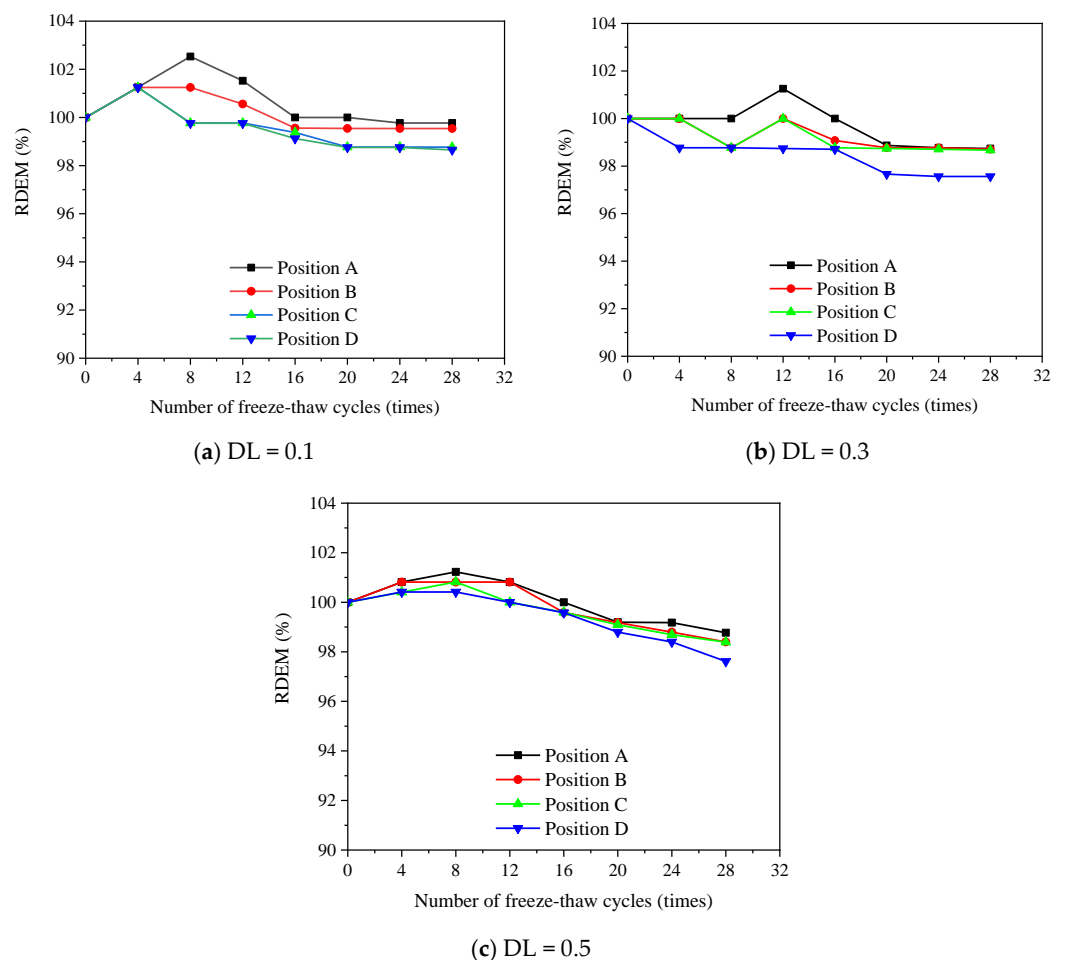


Figure 7. Measured transversal RDEM for specimens under different DL and FCTs subjected to 1% salt solution.

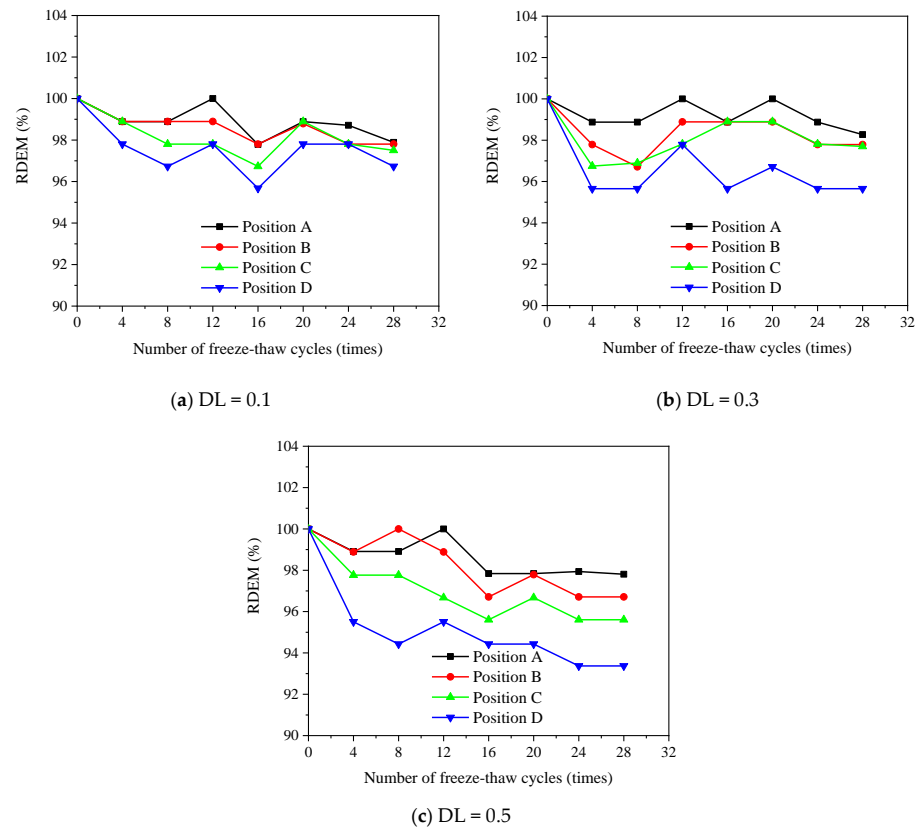


Figure 8. Measured transversal RDEM for specimens under different DL and FCTs subjected to 3% salt solution.

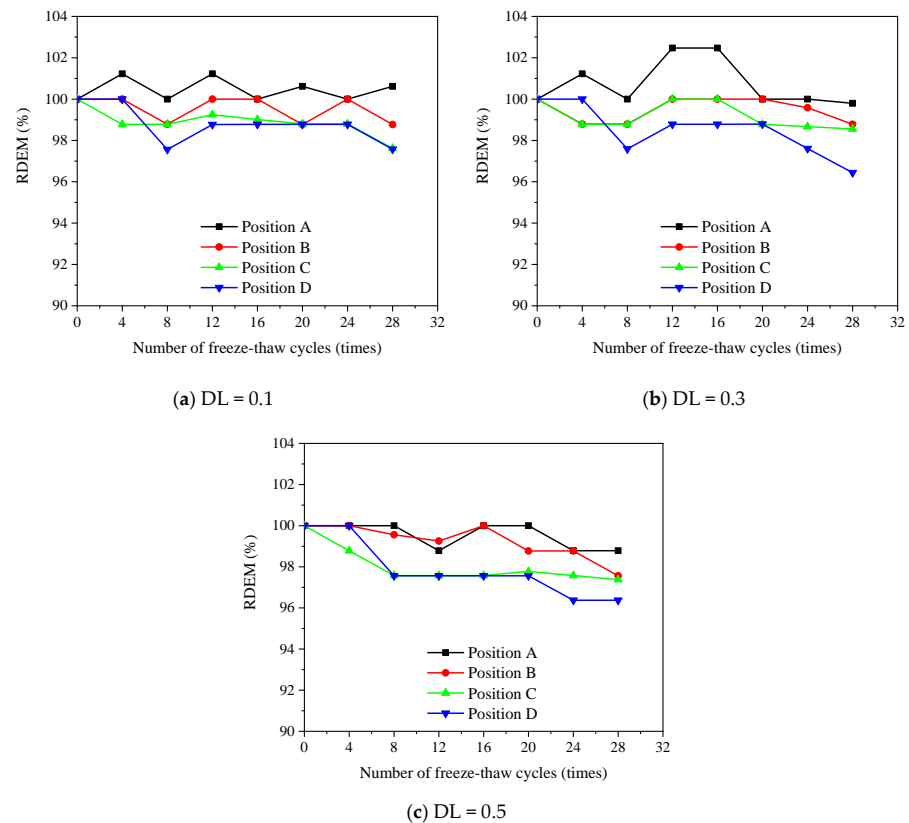


Figure 9. Measured transversal RDEM for specimens under different DL and FCTs subjected to 5% salt solution.

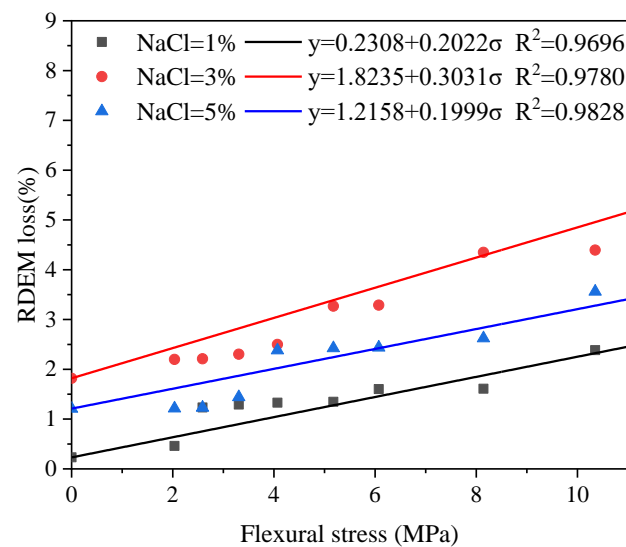


Figure 10. Influence of local flexural stress on the transversal RDEM loss.

3.4. Chloride Penetration Depth

Figure 11a–c plots the measured chloride penetration depth at various positions after 28 FTCs. Regardless of the de-ice salt concentration, the further from the support, the higher penetration depth is observed. This can be attributed to the fact that the area further from the support is under greater sustained local stress level. Combined with the FTCs, more microcracks are created in the area under higher sustained stress. At the support, no significant change is found between specimens under different load levels. This indicates that the shear force at the plane has little contribution to the chloride ingress from the exposed surface. When the deflection level is 0.1 (stress level = 0.59), no significant increase is observed for all cases. This does not hold once the DL reaches 0.3. In terms of 1% NaCl solution, the penetration depth increases from 2.28 mm to 2.52 mm when the deflection level grows from 0.1 to 0.3 at the pure bending zone. The penetration depth increases to 2.83 mm when DL = 0.5.

When the chloride concentration is above 3%, no significant increment on the chloride penetration depth is observed. Specifically, at the position under zero flexural stress, the penetration depths are 2.08, 2.80 and 2.83 mm for 1%, 3% and 5% de-ice salt solution, respectively. Only 1% increment is observed when de-ice salt concentration increases from 3% to 5%, while the increment is 34% between 1% and 3% concentration. A more remarkable increase is observed when deflection is applied. The penetration depth for DL = 0.5 is 2.83 mm for 1% de-ice salt solution. It grows up to 5.51 mm and 6.06 mm for 3% and 5% de-ice salt solution with 94.7% and 114.1% increment, respectively. When no load is applied, the chloride penetration depth after 28 FTCs using 5% NaCl solution is comparable with the one after 11 dry and wet cycles using the same salt solution [51].

Figure 12 presents the evolution of chloride penetration depth with the flexural stress level. An exponential equation was prepared to describe the relationship between them:

$$D = be^{c\sigma} \quad (2)$$

Here, D is the penetration depth of chloride (mm), σ is the flexural stress (MPa) and b and c are the fitting parameters. Parameter b represents the penetration depth under no load and c is used to represent the influence of flexural stress. The exponential equation shows satisfactory fitting results with determination coefficients higher than 0.9. Significant increment is observed for b and c when the salt concentration increases from 1% to 3%, while no big difference is found between 3% and 5% salt concentrations. It is worth mentioning that crack width becomes much larger with increasing the load level, the chloride may penetrate from the side of the crack. Therefore, the proposed relationship

may not work. Nevertheless, the stress level has reached about 0.9 of the load capacity of the materials, which would merely happen for the structural design.

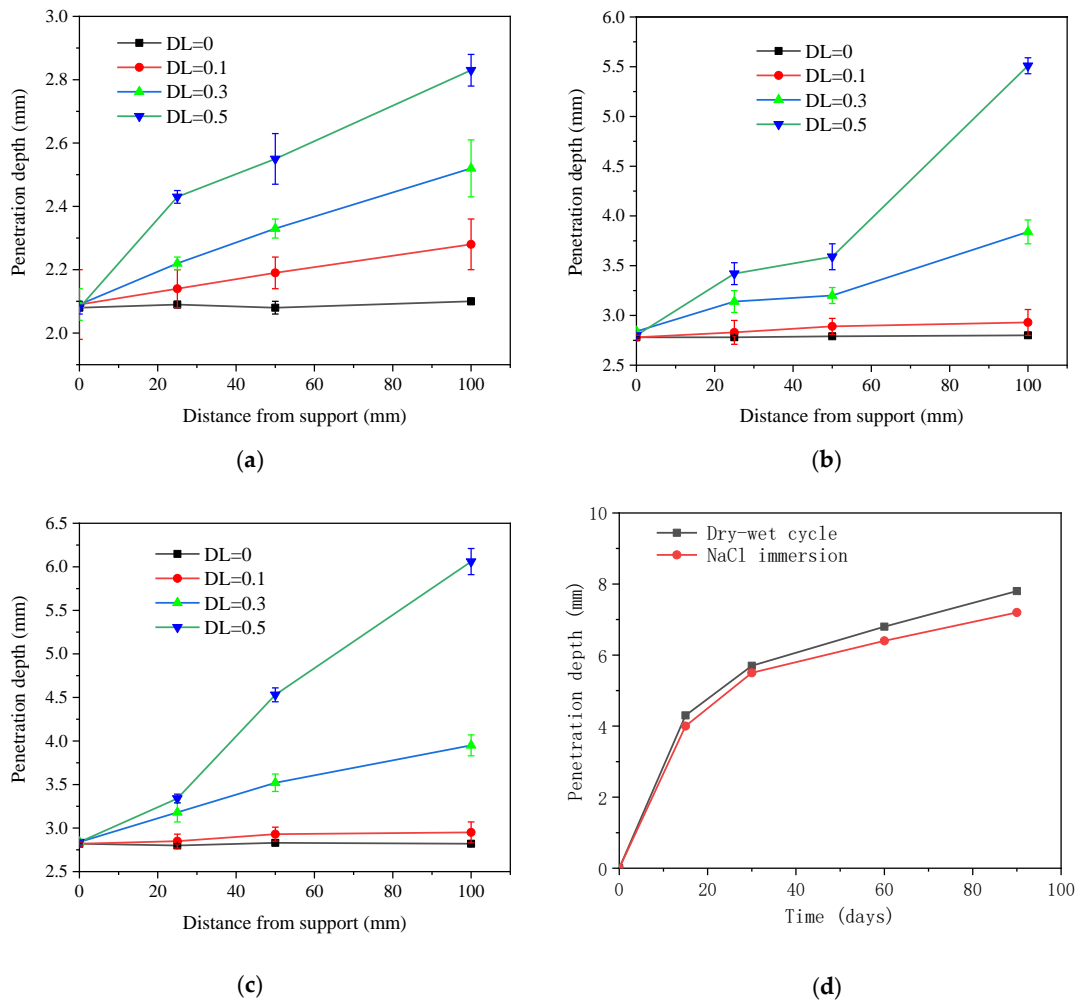


Figure 11. Chloride penetration depth after 28 FCTs under various conditions. (a) 1% NaCl, (b) 3% NaCl, (c) 5% NaCl, (d) Chloride penetration depth in 5% NaCl solution [51].

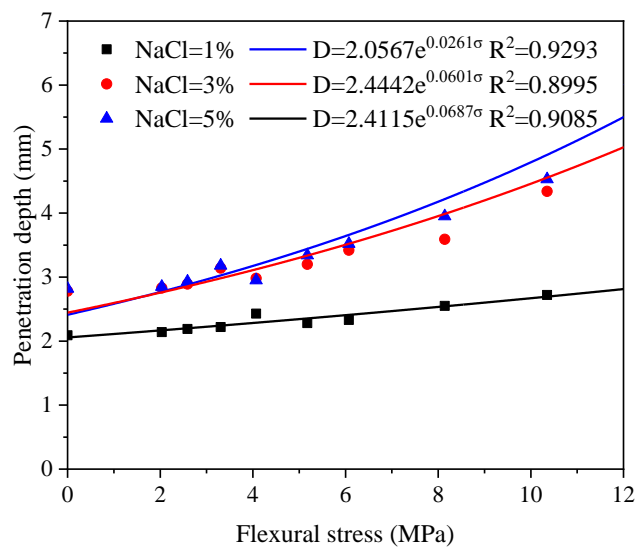


Figure 12. Evolution of chloride penetration depth along flexural stress level after 28 FCTs.

3.5. Free Chloride Content Profile

Figure 13 shows the free chloride content profile in the pure bending zone. The content of free chloride decreases with the depth perpendicular to the exposed surface and the slope becomes gentler. In terms of 1% salt concentration, the free chloride content is 0.22%, 0.26%, 0.28% and 0.32% under different deflection levels at 0–5 mm depth, respectively. The increments are 18.1%, 27.3% and 45.5% for DL = 0.1, 0.3 and 0.5, respectively, compared with DL = 0.

The free chloride content at a depth of 0–5 mm does not show significant difference between the 3% and 5% de-ice salt solutions. The free chloride content is 1.29% and 1.48% for 3% and 5% de-ice salt solutions under no load, respectively. It increases to 1.96% and 1.95% for the 3% and 5% de-ice salt solutions when DL = 0.5, respectively. Regarding the depth of 15–20 mm, when no load is applied the free chloride content for 3% salt solution is smaller than that of 5% salt solution. Once the DL is applied, the free chloride content for 3% salt solution is higher than 5% salt solution. The difference increases with the DL. Specifically, it is 6.25%, 10.53% and 22.2%, for DL = 0.1, 0.3 and 0.5, respectively.

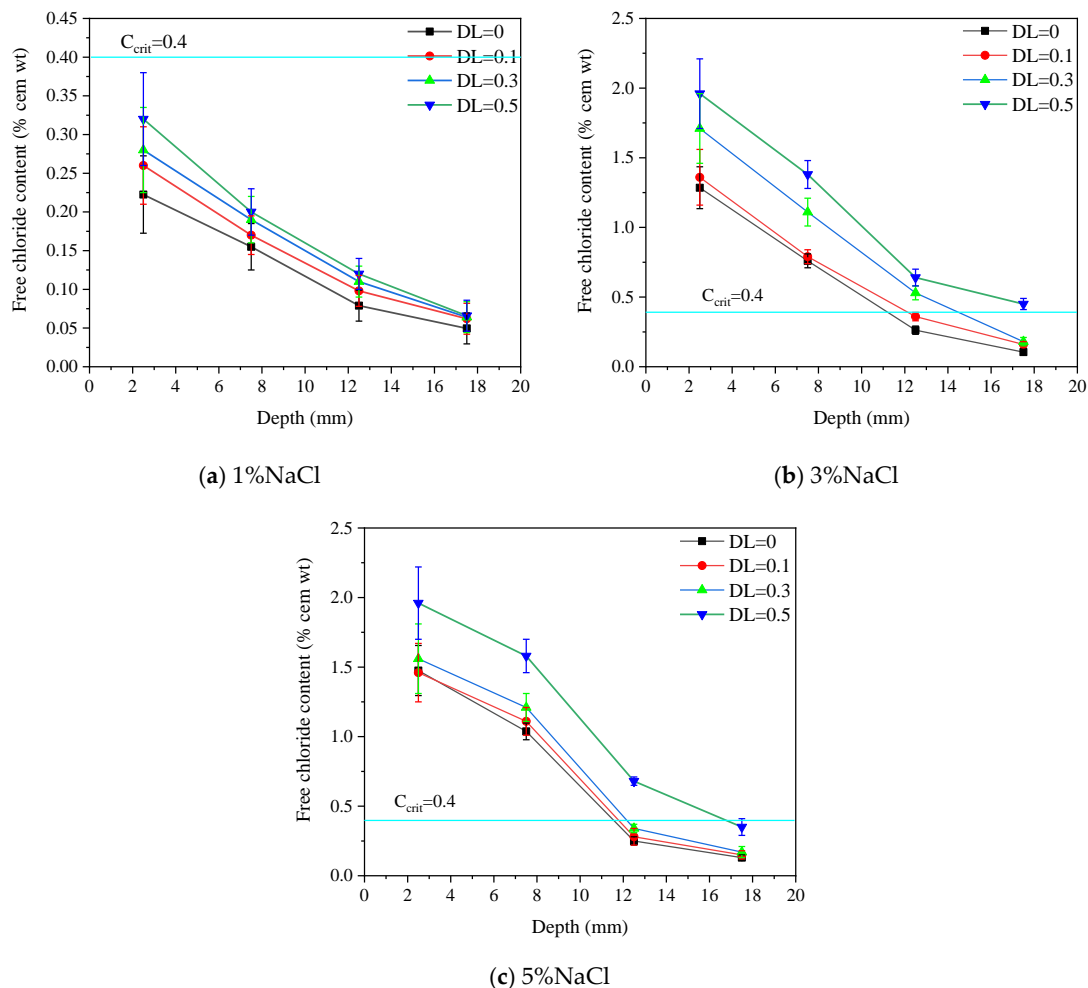


Figure 13. Free chloride ion content after 28 FTCs under various conditions.

The critical chloride content (C_{crit}) is generally considered as 0.4% by the weight of cement (% cem wt) in Europe and North America [52], although other values, e.g., 0.2% cem wt and 0.6% cem wt are also considered [53]. Herein, 0.4% cem wt is used as the key values of the steel [54,55]. Clearly, no depassivation of the steel is expected, even under a large deflection level, when subjected to FTCs under 1% de-ice salt solution. In terms of 5% salt solution, the thickness of cover should be no less than 20 mm when DL = 0.5 is applied.

This does not apply for the 3% salt solution as more serious deterioration occurs in such a concentration. Nevertheless, when $DL < 0.3$, no depassivation of the steel at a depth of 20 mm is expected within 28 FCTs.

4. Conclusions

In this paper, the effect of coupled salt frost attack and sustained load on ECC was investigated. The loss of RDEM, along with the FTCs and chloride penetration depth and free chloride content after 28 FCTs, was measured. The conclusions are as follows.

1. Both the sustained load and salt concentration (no more than 5%) result in higher fluid absorption. The water absorption distributes in the range of 600–1800 g/m². The increment rate decreases with the salt concentration.
2. A 3% NaCl solution leads to the largest deterioration under salt frost with or without load. A linear relationship can be used to describe the relationship between locally sustained flexural stress and RDEM loss after FTCs. The load level is most significant on the RDEM loss in 3% NaCl solution (i.e., the pessimum concentration). The RDEM loss rate in the 3% NaCl solution is almost 50% greater than others.
3. The chloride penetration depth increases with the locally sustained flexural stress. A significant increment of chloride penetration depth is observed when salt concentration increases from 1% to 3%. Almost 100% increment occurs in the pure bending zone, while no big difference is found between 3% and 5% salt concentrations.
4. After FTCs, the free chloride content at a depth of 0–5 mm does not show remarkable difference for the 3% and 5% salt solutions. Regarding depth of 15–20 mm, when no load is applied, the free chloride content for 3% salt solution is smaller than that of 5% salt solution. Once the sustained load is applied, the free chloride content for 3% salt solution is higher than the 5% salt solution. The difference increases with the DL.
5. When the ECC is subjected to the FTCs under 1% de-ice salt solution, no depassivation of the steel is expected even under a large deflection level. In terms of 3% and 5% salt solution, the thickness of cover should be no less than 20 mm when $DL = 0.5$ is applied.

The behavior of ECCs subjected to the coupled sustained flexural load and salt frost was investigated, albeit limited to the meso-scale. Further studies, including the change of the microstructure and chemical phases at the micro-scale, are required.

Author Contributions: Methodology, R.S., Y.L. (Yifeng Ling) and B.Š.; Software, C.T.; Investigation, Y.L. (Yonghao Li) and C.T.; Writing—original draft, Y.L. (Yonghao Li); Writing—review & editing, Y.G., H.Z. and B.Š.; Data curation, N.Z.; Formal analysis, L.L.; Visualization, Y.L. (Yifeng Ling); Supervision, R.S.; Funding acquisition, N.Z. and L.L. All authors have read and agreed to the published version of the manuscript.

Funding: This work was supported by the National Natural Science Foundation of China (No. 52008234), Taishan Scholars Foundation of Shandong Province (No. tsqn201909032), Natural Science Foundation of Jiangsu Province (No. BK20200235) and Natural Science Foundation of Shandong Province (ZR2021QE174, ZR2021ME215).

Institutional Review Board Statement: Not applicable.

Informed Consent Statement: Not applicable.

Data Availability Statement: The data presented in this study are available upon request from the corresponding author.

Acknowledgments: Sincere thanks to the research laboratory of Qilu Transportation, Shandong University.

Conflicts of Interest: The authors declare no conflict of interest.

References

1. Bentur, A.; Mindess, S. *Fibre Reinforced Cementitious Composites*; CRC Press: Boca Raton, FL, USA, 2006.
2. Van Zijl, G.P.A.G.; Wittmann, F.H. On Durability of SHCC. *J. Adv. Concr. Technol.* **2010**, *8*, 261–271. [[CrossRef](#)]
3. Li, H.D.; Xu, S.L.; Leung, C.K.Y. Tensile and flexural properties of ultra high toughness cementitious composite. *J. Wuhan Univ. Technol. Mater. Sci. Ed.* **2009**, *24*, 677–683. [[CrossRef](#)]
4. Moradi, N.; Taviana, M.H.; Habibi, M.R.; Amiri, M.; Moradi, M.J.; Farhangi, V.J.M. Predicting the Compressive Strength of Concrete Containing Binary Supplementary Cementitious Material Using Machine Learning Approach. *Materials* **2022**, *15*, 5336. [[CrossRef](#)] [[PubMed](#)]
5. Shanmugasundaram, N.; Praveenkumar, S.J.C. Influence of supplementary cementitious materials, curing conditions and mixing ratios on fresh and mechanical properties of engineered cementitious composites—A review. *Constr. Build. Mater.* **2021**, *309*, 125038. [[CrossRef](#)]
6. Farhangi, V.; Karakouzian, M.J.A.S. Effect of fiber reinforced polymer tubes filled with recycled materials and concrete on structural capacity of pile foundations. *Appl. Sci.* **2020**, *10*, 1554. [[CrossRef](#)]
7. Suthiwarapirak, P.; Matsumoto, T.; Kanda, T. Multiple cracking and fiber bridging characteristics of engineered cementitious composites under fatigue flexure. *J. Mater. Civ. Eng.* **2004**, *16*, 433–443. [[CrossRef](#)]
8. Qian, S.Z.; Zhou, J.; Schlangen, E. Influence of curing condition and precracking time on the self-healing behavior of Engineered Cementitious Composites. *Cem. Concr. Compos.* **2010**, *32*, 686–693. [[CrossRef](#)]
9. Yang, Y.; Yang, E.-H.; Li, V.C. Autogenous healing of engineered cementitious composites at early age. *Cem. Concr. Res.* **2011**, *41*, 176–183. [[CrossRef](#)]
10. Zhao, Y.J.; Jiang, J.W.; Ni, F.J.; Zhou, L. Fatigue Cracking Resistance of Engineered Cementitious Composites (ECC) under Working Condition of Orthotropic Steel Bridge Decks Pavement. *Appl. Sci.* **2019**, *9*, 3577. [[CrossRef](#)]
11. Guan, Y.H.; Wu, J.J.; Sun, R.J.; Zhang, H.Z.; Hu, Y.Q.; Wang, F. Transverse Flexural Behaviour of Steel-Engineering Cementitious Composites (ECC) Composite Deck under Negative and Positive Bending Forces. *KSCE J. Civ. Eng.* **2021**, *25*, 2962–2973. [[CrossRef](#)]
12. Zhang, J.; Li, V.C. Monotonic and fatigue performance in bending of fiber-reinforced engineered cementitious composite in overlay system. *Cem. Concr. Res.* **2002**, *32*, 415–423. [[CrossRef](#)]
13. Mustafa, S.; Singh, S.; Hordijk, D.; Schlangen, E.; Luković, M. Experimental and numerical investigation on the role of interface for crack-width control of hybrid SHCC concrete beams. *Eng. Struct.* **2022**, *251*, 113378. [[CrossRef](#)]
14. Luković, M.; Hordijk, D.; Huang, Z.; Schlangen, E. Strain Hardening Cementitious Composite (SHCC) for crack width control in reinforced concrete beams. *Heron* **2019**, *64*, 181.
15. Huang, B.T.; Li, Q.H.; Xu, S.L.; Zhang, L. Static and fatigue performance of reinforced concrete beam strengthened with strain-hardening fiber-reinforced cementitious composite. *Eng. Struct.* **2019**, *199*, 109576. [[CrossRef](#)]
16. Sahmaran, M.; Li, M.; Li, V.C. Transport properties of engineered cementitious composites under chloride exposure. *ACI Mater. J.* **2007**, *104*, 604–611.
17. Lepech, M.D.; Li, V.C. Water permeability of engineered cementitious composites. *Cem. Concr. Compos.* **2009**, *31*, 744–753. [[CrossRef](#)]
18. Ng, K.; Sun, Y.; Dai, Q.L.; Yu, X. Investigation of internal frost damage in cementitious materials with micromechanics analysis, SEM imaging and ultrasonic wave scattering techniques. *Constr. Build. Mater.* **2014**, *50*, 478–485. [[CrossRef](#)]
19. Sutter, L.; Peterson, K.; Julio-Betancourt, G.; Hooton, D.; Dam, T.V.; Smith, K. *The Deleterious Chemical Effects of Concentrated Deicing Solutions on Portland Cement Concrete*; South Dakota Department of Transportation, Office of Research: Pierre, SD, USA, 2008.
20. Pigeon, M. *Durability of Concrete in Cold Climates*; CRC Press: Boca Raton, FL, USA, 2014.
21. Valenza, J.J., II; Scherer, G.W. A review of salt scaling: I. Phenomenology. *Cem. Concr. Res.* **2007**, *37*, 1007–1021. [[CrossRef](#)]
22. Amini, K. *Toward Salt-Scaling Resistant Concrete*; Iowa State University: Iowa City, IA, USA, 2018.
23. Scherer, G.W. Crystallization in pores. *Cem. Concr. Res.* **1999**, *29*, 1347–1358. [[CrossRef](#)]
24. Valenza, J.J.; Scherer, G.W. A Review of Salt Scaling: II. Mechanisms. *Cem. Concr. Res.* **2007**, *37*, 1022–1034, Erratum in *Cem. Concr. Res.* **2019**, *116*, 70. [[CrossRef](#)]
25. Shi, X.M.; Fay, L.; Peterson, M.M.; Berry, M.; Mooney, M. A FESEM/EDX investigation into how continuous deicer exposure affects the chemistry of Portland cement concrete. *Constr. Build. Mater.* **2011**, *25*, 957–966. [[CrossRef](#)]
26. Shi, X.; Akin, M.; Pan, T.; Fay, L.; Liu, Y.; Yang, Z.J. Deicer impacts on pavement materials: Introduction and recent developments. *Open Civ. Eng. J.* **2009**, *3*, 16–27. [[CrossRef](#)]
27. Li, Y.X.; Fang, Y.D.; Seeley, N.; Jungwirth, S.; Jackson, E.; Shi, X.M. Corrosion by Chloride Deicers on Highway Maintenance Equipment Renewed Perspective and Laboratory Investigation. *Transp. Res. Rec.* **2013**, *2361*, 106–113. [[CrossRef](#)]
28. Liu, Y.S.; Zhou, X.M.; Lv, C.B.; Yang, Y.Z.; Liu, T.A. Use of Silica Fume and GGBS to Improve Frost Resistance of ECC with High-Volume Fly Ash. *Adv. Civ. Eng.* **2018**, *2018*. [[CrossRef](#)]
29. Nam, J.; Kim, G.; Lee, B.; Hasegawa, R.; Hama, Y. Frost resistance of polyvinyl alcohol fiber and polypropylene fiber reinforced cementitious composites under freeze thaw cycling. *Compos. Part B Eng.* **2016**, *90*, 241–250. [[CrossRef](#)]
30. van Zijl, G.P.A.G.; Wittmann, F.H.; Oh, B.H.; Kabele, P.; Toledo Filho, R.D.; Fairbairn, E.M.R.; Slowik, V.; Ogawa, A.; Hoshiro, H.; Mechtcherine, V.; et al. Durability of strain-hardening cement-based composites (SHCC). *Mater. Struct.* **2012**, *45*, 1447–1463. [[CrossRef](#)]

31. Şahmaran, M.; Li, V.C. De-icing salt scaling resistance of mechanically loaded engineered cementitious composites. *Cem. Concr. Res.* **2007**, *37*, 1035–1046. [[CrossRef](#)]
32. Yin, L.; Yan, C.; Liu, S. Freeze–Thaw Durability of Strain-Hardening Cement-Based Composites under Combined Flexural Load and Chloride Environment. *Materials* **2018**, *11*, 1721. [[CrossRef](#)]
33. Ge, Z.; Tawfek, A.M.; Zhang, H.Z.; Yang, Y.W.; Yuan, H.Q.; Sun, R.J.; Wang, Z. Influence of an extrusion approach on the fiber orientation and mechanical properties of engineering cementitious composite. *Constr. Build. Mater.* **2021**, *306*, 124876. [[CrossRef](#)]
34. Sun, R.; Han, L.; Zhang, H.; Ge, Z.; Guan, Y.; Ling, Y.; Schlangen, E.; Šavija, B. Fatigue life and cracking characterization of engineered cementitious composites (ECC) under flexural cyclic load. *Constr. Build. Mater.* **2022**, *335*, 127465. [[CrossRef](#)]
35. Zhang, W.; Pi, Y.; Kong, W.; Zhang, Y.; Wu, P.; Zeng, W.; Yang, F. Influence of damage degree on the degradation of concrete under freezing-thawing cycles. *Constr. Build. Mater.* **2020**, *260*, 119903. [[CrossRef](#)]
36. Otsuki, N.; Nagataki, S.; Nakashita, K. Evaluation of AgNO₃ solution spray method for measurement of chloride penetration into hardened cementitious matrix materials. *Mater. J.* **1992**, *89*, 587–592.
37. Słomka-Słupik, B.; Podwórny, J.; Staszuk, M. Corrosion of cement pastes made of CEM I and CEM III/A caused by a saturated water solution of ammonium chloride after 4 and 25 days of aggressive immersion. *Constr. Build. Mater.* **2018**, *170*, 279–289. [[CrossRef](#)]
38. Šavija, B.; Luković, M.; Schlangen, E. Influence of Cracking on Moisture Uptake in Strain-Hardening Cementitious Composites. *J. Nanomechanics Micromechanics* **2017**, *7*. [[CrossRef](#)]
39. Qiu, W.L.; Teng, F.; Pan, S.S. Damage constitutive model of concrete under repeated load after seawater freeze-thaw cycles. *Constr. Build. Mater.* **2020**, *236*, 117560. [[CrossRef](#)]
40. Yang, Q. One of mechanisms on the deicer–frost scaling of concrete (II): Degree of saturation and ice-formation pressure during freezing-thawing cycles. *J. Build. Mater* **2012**, *6*, 741–746.
41. Yu, J.; Gao, S.; Hou, D.; Wang, P.; Sun, G. Water Transport Mechanisms of Poly(acrylic acid), Poly(vinyl alcohol), and Poly(ethylene glycol) in C-S-H Nanochannels: A Molecular Dynamics Study. *J. Phys. Chem. B* **2020**, *124*, 6095–6104. [[CrossRef](#)]
42. Al-Kutti, W.; Nasir, M.; Johari, M.A.M.; Islam, A.B.M.S.; Manda, A.A.; Blaisi, N.I. An overview and experimental study on hybrid binders containing date palm ash, fly ash, OPC and activator composites. *Constr. Build. Mater.* **2018**, *159*, 567–577. [[CrossRef](#)]
43. Heravi, A.A.; Mosig, O.; Tawfik, A.; Curbach, M.; Mechtcherine, V. An experimental investigation of the behavior of strain-hardening cement-based composites (SHCC) under impact compression and shear loading. *Materials* **2020**, *13*, 4514. [[CrossRef](#)]
44. Romero Rodríguez, C.; França de Mendonça Filho, F.; Chaves Figueiredo, S.; Schlangen, E.; Šavija, B. Fundamental investigation on the frost resistance of mortar with microencapsulated phase change materials. *Cem. Concr. Compos.* **2020**, *113*, 103705. [[CrossRef](#)]
45. Gong, F.Y.; Takahashi, Y.; Segawa, I.; Maekawa, K. Mechanical properties of concrete with smeared cracking by alkali-silica reaction and freeze-thaw cycles. *Cem. Concr. Compos.* **2020**, *111*, 103623. [[CrossRef](#)]
46. Zhang, P.; Dai, Y.Q.; Ding, X.Y.; Zhou, C.S.; Xue, X.; Zhao, T.J. Self-healing behaviour of multiple microcracks of strain hardening cementitious composites (SHCC). *Constr. Build. Mater.* **2018**, *169*, 705–715. [[CrossRef](#)]
47. Çopuroğlu, O.; Schlangen, E. Modeling of frost salt scaling. *Cem. Concr. Res.* **2008**, *38*, 27–39. [[CrossRef](#)]
48. He, Z.; Tang, S.W.; Zhao, G.S.; Chen, E. Comparison of three and one dimensional attacks of freeze-thaw and carbonation for concrete samples. *Constr. Build. Mater.* **2016**, *127*, 596–606. [[CrossRef](#)]
49. Chuang, W.; Geng-sheng, J.; Bing-liang, L.; Lei, P.; Ying, F.; Ni, G.; Ke-zhi, L. Dispersion of carbon fibers and conductivity of carbon fiber-reinforced cement-based composites. *Ceram. Int.* **2017**, *43*, 15122–15132. [[CrossRef](#)]
50. Wu, Z.; Shi, C.; Gao, P.; Wang, D.; Cao, Z. Effects of deicing salts on the scaling resistance of concrete. *J. Mater. Civ. Eng.* **2015**, *27*, 04014160. [[CrossRef](#)]
51. Sun, R.; Hu, X.; Ling, Y.; Zuo, Z.; Zhuang, P.; Wang, F. Chloride diffusion behavior of engineered cementitious composite under dry-wet cycles. *Constr. Build. Mater.* **2020**, *260*, 119943. [[CrossRef](#)]
52. Angst, U.; Elsener, B.; Larsen, C.K.; Vennesland, Ø. Critical chloride content in reinforced concrete—A review. *Cem. Concr. Res.* **2009**, *39*, 1122–1138. [[CrossRef](#)]
53. Schießl, P.; Bamforth, P.; Baroghel-Bouny, V.; Corley, G.; Faber, M.; Forbes, J.; Gehlen, C.; Helene, P.; Helland, S.; Ishida, T.; et al. *Model Code for Service Life Design*; fib bulletin No. 34; International Federation for Structural Concrete: Lausanne, Switzerland, 2006.
54. Ghanem, H.; Phelan, S.; Senadheera, S.; Pruski, K. Chloride ion transport in bridge deck concrete under different curing durations. *J. Bridg. Eng.* **2008**, *13*, 218–225. [[CrossRef](#)]
55. Ghanem, H.; Trad, A.; Dandachy, M.; Elkordi, A. Effect of Wet-Mat Curing Time on Chloride Permeability of Concrete Bridge Decks. In *International Congress and Exhibition “Sustainable Civil Infrastructures: Innovative Infrastructure Geotechnology”*; Springer: Berlin/Heidelberg, Germany, 2018; pp. 194–208.

Disclaimer/Publisher’s Note: The statements, opinions and data contained in all publications are solely those of the individual author(s) and contributor(s) and not of MDPI and/or the editor(s). MDPI and/or the editor(s) disclaim responsibility for any injury to people or property resulting from any ideas, methods, instructions or products referred to in the content.